Proceedings of ASME Turbo Expo 2011
GT2011
June 6-10, 2011, Vancouver, British Columbia, Canada

GT2011-45495

SIMULATION OF BLADE CASING INTERACTION PHENOMENA IN GAS TURBINES RESULTING FROM HEAVY TIP RUBS USING AN IMPLICIT TIME MARCHING METHOD

Robin J Williams
Design Systems & Mechanical Methods ML-78
Rolls-Royce plc
Derby, DE24 8BJ, UK

ABSTRACT

Severe rubs between gas turbine blades and engine casings can in extreme cases result in damaging blade vibration levels and rapid loss of casing lining material. Even for more minor rubs, the wear in the lining material will result in increase tip gaps and a consequent loss in efficiency. Major rub events are extremely rare in practice, and there is seldom any useful diagnostic evidence of the root cause of the behaviour. Moreover, traditional analysis methods are not suitable for exploring the wide range of potential conditions under which an unstable vibration response might be initiated.

A new modelling technique has been developed for modelling blade casing rubs which includes a detailed model of the interaction with liner wear. The method is time based, but is very efficient, enabling a wide range of initiating conditions to be explored. A series of examples have been developed to firstly: demonstrate the method is robust and reliable, and secondly: to investigate potential interaction phenomena under representative simulated conditions. The method has been applied to a real blade example, for which severe wear is known to have occurred. The method predicts that instability may occur above a threshold level of tip rub severity, and also demonstrates the improvement in an alternative blade design for which rub tolerance is known to be superior.

INTRODUCTION

The contact forces resulting from high-speed intermittent rubs between gas turbine rotor blades and engine casing linings may induce transient aerofoil vibration. This will modulate the contact forces at a frequency which is synchronous with the blade natural vibration frequencies, and in extreme cases, an unstable or limit cycle vibration response may result. This is characterised by heavy wear in the liner material that may be deeper than the nominal incursion depth, and the wear pattern may also be circumferentially periodic. This phenomena falls outside the scope of traditional engine rotordynamics analyses and aerofoil forced response analyses where the whole engine and aerofoil dynamic behaviour are considered independently. Detailed coupled casing and blade models using explicit Finite Element Methods are used for blade release impact simulations, but these models are generally too computationally expensive to run for the timescales required for the dynamic response to become fully developed.

In recent years there has been considerable interest in the measurement and prediction of tip rub phenomena. In particular, a highly developed test facility is described in [1], which enables the response to repeated short duration intense rubs to be measured. Corresponding numerical modelling of the casing response to moving loads is described in [2] and the contact stiffness properties of rubbing blades is developed in [3]. However, while this and other research addresses the component parts of blade casing interaction in much more detail than is presented here, the entire dynamic system has not been assembled to the level necessary to enable self-sustaining dynamic response behaviour to be predicted.

Traditionally within Rolls-Royce, detailed FE models of gas turbine engines are heavily reduced for dynamics and vibration analysis, where the reduction is usually achieved using the Component Mode Synthesis (CMS) method [4]. The rotors are generally reduced to a centreline only representation, and the effects of rotation are restricted to gyroscopic force terms applied to the rotor axis. This methodology has been extended, while retaining the basic centre-line rotor configuration, to enable the interaction between individual blades and the casing to be simulated. Discrete stationary reduced FE models of individual blades are processed concurrently with an engine

rotordynamics model. The interaction between the blades and the casing is modelled by repeatedly transforming and exchanging local displacements and forces between the rotating and stationary coordinate frames. The blade tip vibration is added to the rotor motion to obtain more representative incursion depths, and the resulting friction and wear forces are applied to the blade tips to induce representative deflection and transient response behaviour. In addition, a non-FE eroding model of the casing liner material is included which has representative friction and localised wear properties.

Using this approach, it has been possible to simulate complex blade casing interaction phenomena. As the engine and blade modes are massively reduced, but retain representative dynamic characteristics, the process is computationally very efficient and it is therefore possible to simulate representative sweep rates through resonance conditions. Conditions under which the onset of wear-induced instability may occur can be predicted, and have been shown to be influenced by the detailed modeshapes of the fundamental aerofoil vibration modes.

SOLVER DESCRIPTION

The models described in this paper are solved using a Rolls-Royce proprietary implicit time marching method with continuously variable time step adaptation, which is similar conceptually to the Nastran NLTRAN (Solution Sequence 129) non-linear transient method. The method is conventionally used for modelling non-linear rotordynamics phenomena for whole engine and aircraft simulations using large structural models, but the method is also adaptable for much smaller scale research studies [5].

The input models are linear mass and stiffness matrices that have been dynamically reduced using an independent FEA package (generally Nastran, but reduced models generated using other Rolls-Royce proprietary software are also used). A variety of custom designed non-linear elements have been developed which interact with the linear model by applying time dependent external forces at discrete points in the structure. Internal to the solver the equations of motion are configured in the form

$$M\ddot{q} + kq = p(t) + f(\ddot{q}, \dot{q}, q, t) \qquad (1)$$

where M and k are the linear system mass and stiffness matrices, q is a vector of system displacements, p is a vector of external time dependent loads, and f is a vector of response and load dependent forces, as determined using the various non-linear interaction elements available. A damping matrix is not specifically included in the system model, but damping is represented by a vector of linear velocity dependent forces in the vector of interaction forces (f).

The implicit time marching solver has been optimised to converge efficiently for the special case where the structure is inherently linear, but with localised non-linearity. This enables point plasticity to be modelled for example, but the method is not suitable for more general non-linear material properties, where the left hand side of the system equations (1) would change with load, and an alternative method would be more appropriate, but would result in longer solution times. However, although the speed and robustness of the solver is beneficial, the principal advantage of using the method is that it enables highly specific non-linear interaction features to be modelled to a much higher level of detail than is possible using a commercially available FE package, and the blade casing interaction studies described here, are heavily dependent on the bespoke capabilities summarised in the following sections.

The solver works exclusively in the time domain, but an equivalent multi-harmonic balance frequency domain method has been developed by Dr. E. Petrov at Imperial College, UK [6], which has a similar range of application elements. The frequency domain solver is much faster for steady state phenomena, but a time domain solution is more appropriate where transient or load dependent boundary conditions occur.

DEVELOPMENT OF A SNUBBING MODEL

At the heart of the method is a simple model for annular snubbing, which in its most basic form is similar to that used in other FEA codes. The displacement at a reference rotor location is compared with that of an equivalent casing location, and if the relative displacement exceeds the radial clearance then contact is deemed to have occurred, and opposing contact and friction forces are applied to the rotor and stator.

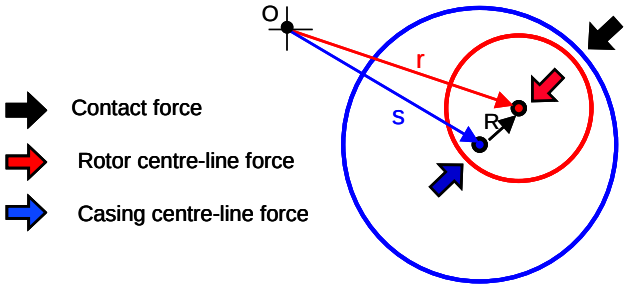

Fig 1: Centreline Rotor Casing Snub Model

In its most basic form, the rotor and stator may be reduced to single centreline nodes (Fig 1), and the contact forces are then calculated using the equations.

$$R_{r-s} = \sqrt{(x_r - x_s)^2 + (y_r - y_s)^2} \qquad (2)$$

$$R_i = R_{r-s} - c \qquad (3)$$

$$F_R = k \cdot R_i \ , \quad F_T = \mu \cdot F_R \qquad (4 \ \& \ 5)$$

$$F_{xr} = -F_R \cdot \frac{(x_r - x_s)}{R_i} + F_T \cdot \frac{(y_r - y_s)}{R_i} \qquad (6)$$

$$F_{yr} = -F_R \cdot \frac{(y_r - y_s)}{R_i} + F_T \cdot \frac{(x_r - x_s)}{R_i} \qquad (7)$$

where x and y are the in-plane Cartesian displacement directions, R and T are the equivalent Cylindrical directions, c is the nominal clearance, k is the contact stiffness, F is the contact

force, μ is the Coulomb friction coefficient and the subscripts *r*, *s*, and *i*, refer to rotor, stator, and incursion specific properties respectively.

The contact forces are calculated assuming Coulomb friction and linear contact stiffness. Typically, the radial stiffness of the rotor will be much lower than that of the stator - due to the flexibility of the blades, and the contact stiffness can be chosen to be representative of the blade radial stiffness. This contact model is equivalent to the NLRGAP element in NASTRAN and is widely used for modelling snubs in turbomachinery. The formulation is limited however, as it does not account for the localised flexibility of the casing, or the changes in the net radial stiffness of the contact which occur as different numbers of blades come into contact.

Enhanced Snubbing Model

The basic centreline contact model described above is enhanced to include the effects of casing flexibility, and the effects of multiple rotating blades, while retaining the annular contact model for calculating the contact forces. For this approach, the casing is not reduced to a single centreline node, but is reduced to a ring of nodes in the plane of the contact. The rotor is maintained as a centre-line reference node, but the contact forces are calculated assuming the presence of virtual rotating blades. Each blade is represented by a rotating spring, the stiffness of which is representative of the radial stiffness of an individual blade – Fig 2.

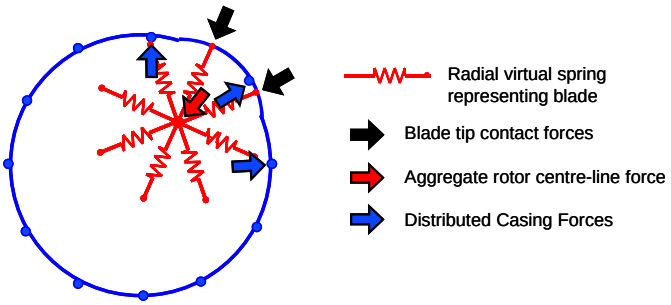

Fig 2: Multi-blade/Flexible casing Snub Model

These spring elements are virtual, and are not included in the input FE model. The blades are considered to rotate at the defined speed of the rotor, and as such, the angular position of each blade can be determined at any point in time, and contact with the casing may only occur at these moving angular positions. The free radial displacement of a blade is found by resolving the net rotor centreline displacement in the radial direction of the blade, and the corresponding radial displacement of the casing is found by interpolation of the nearest pair of casing nodes. The contact forces can then be calculated using the standard annular snubbing calculation (Equations 2-7). For the case of multiple blade contact, the forces on each blade tip are summed at the rotor centreline node, and the casing forces are interpolated onto the nearest pair of casing nodes for each contacting blade. Using this approach, the dynamic behaviour of the casing will be representative of the localised forcing applied by the blades.

This distributed annular snubbing model is the standard contact model used throughout the following analysis, but its behaviour can be modified by inclusion of some of the additional enhancements described below.

Non-linear contact stiffness

The radial stiffness of typical blades is non-linear even in cases where the behaviour remains elastic. Under the action of the tip loading forces, which includes a lateral component due to friction, the blade will deflect both radially and laterally, and the resulting lean of the blade will generally give rise to a reduction in the apparent radial stiffness. This behaviour can only be predicted using a geometrically non-linear static load analysis of a detailed FE blade model. A steadily increasing load is applied to the detailed model at the blade tip at an angle that is inclined relative to the radial direction to represent the effects of friction. The load is applied at a representative rate to ensure that strain rate dependency effects are captured. The increase in radial deflection is obtained as a function of radial load by post-processing the results of the analysis. This detailed FE analysis may be very large, however, it is not necessary to run the detailed model repeatedly and concurrently with the transient analysis. It is only necessary to run the detailed model once in order to determine the load deflection characteristics, which can then be imported into the transient model in the form of a table, or preferably as a smooth spline function. The apparent radial stiffness of the blade will vary with rotor speed due to centrifugal stiffening. The detailed model must therefore be run at representative rotation speed, and if the speed variation is significant, it will be necessary to interpolate using a polynomial function between two bounding speed conditions.

It is preferable to describe non-linear stiffness properties in terms of a load deflection characteristic, instead of a stiffness characteristic as it enables grossly non-linear effects such as plasticity to be included, which may include a falling characteristic beyond the yield condition.

For monotonically increasing loading of a blade, the effects of geometrically non-linear elastic behaviour and plasticity are indistinguishable. However, if the detailed blade model is unloaded from a high load condition, then the difference between the loading and unloading characteristics provides a measure of the reduction in nominal radial length due to plasticity. In practice, the unload characteristic will be different at each starting unload condition, but an approximate estimate of the plasticity at incremental load conditions can be obtained using a single high load unloading characteristic. This is illustrated diagrammatically in Fig 3, where the blue trace represents the loading characteristic and the solid red trace represents the corresponding unloading characteristic. The offset between these characteristics at zero load indicates the accumulated plasticity at the peak load condition. If the intercept of the unload characteristic is re-datumed to the origin (dashed red line) then the difference between this and the load

characteristic is an estimate of the accumulated plasticity at different load conditions (magenta lines). In practice, the offset of the unload characteristic is continually redatumed such that it intercepts the loading characteristic at the peak achieved displacement condition (green lines). The current redatumed unload characteristic will be used to determine the radial load while the displacement is below the peak level – irrespective of whether the displacement is increasing or decreasing, and the loading characteristic (blue line) will be used when the peak displacement is increasing. Fig 3 indicates diagrammatically the load deflection history for a complex cycle comprising three partial unload conditions. In addition to plasticity, the clearance may also be adjusted for load and time dependent blade tip wear.

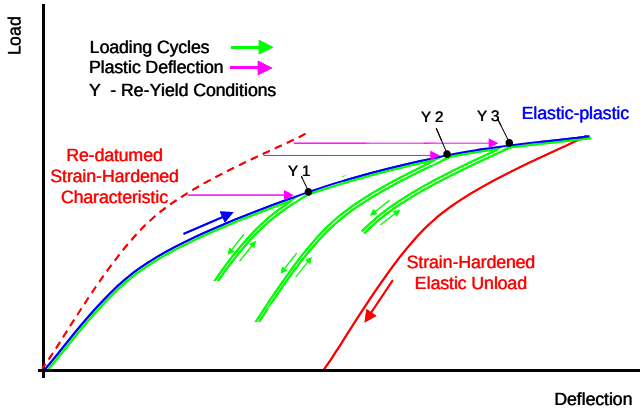

Fig. 3: Blade Radial Plasticity Model

Liner and Casing Wear

The previous section describes how the nominal blade length can be modified to account for the effects of plasticity and wear, and this will change the local clearance used to calculate the snubbing forces for individual blades. In addition to this however, there may be load dependent wear of the casing lining material, which will also affect the local clearance. If the casing is lined with a weak abradable material, then the wear may be considerable. Casing wear will be non-uniform if blade contact is intermittent or periodic, and the casing shape will then no longer be circular, giving rise to periodic variations in the local clearance experienced by rotating blades.

The casing is represented in the snubbing model by an annular array of cells, each having a depth value that is initially set to the nominal depth of the liner material. The liner is not included in the FE model of the casing, and the number of liner cells will typically be much larger than the number of casing nodes. The liner material will in practice offer some resistance to blade incursion, and this can be represented as a non-linear characteristic defining the incursion depth as a function of load. This characteristic may be established using materials testing or through detailed modelling. The characteristic may include an initial zero wear region, if the material does not erode until the load exceeds a threshold value.

In calculating the instantaneous liner incursion depth, consideration must also be given to the non-linear radial stiffness of the blade, as the radial elastic/plastic compression of the blade will reduce the net incursion, i.e.

$$e_{free} = e_{wear} + \Delta e_{wear}(P_r) \cdot \Delta t + e_{blade}(P_r) \quad , \qquad (8)$$

where e_{free} is the free incursion depth, e_{wear} is the cumulative liner wear at the start of the time step, Δe_{wear} is the incremental liner penetration depth and e_{blade} is the radial compression of the aerofoil. Both the radial compression and the incursion depth, will be independent non-linear functions of the transmitted radial load (P_r). An iterative procedure is required to identify the correct $e_{blade} : \Delta e_{wear}$ distribution for which the compressive load is equal to the incursion load (Fig 4B).

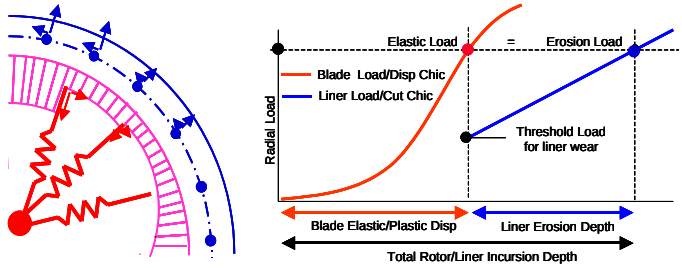

Fig. 4: Liner Wear model & Radial Load Balance

If the incursion depth becomes larger than the local remaining depth of the liner, then direct contact with the casing will occur, and this must be included in the equilibrium load calculation. In this case, the load due to erosion can be calculated directly from the residual depth of the liner, and this can be accounted for as a pre-compression of the blade within the standard blade/casing contact calculation. Once the incursion depth has been established, the removal rate of liner material can be determined due to rotor rotation. The progress of each blade as it passes through individual cells is monitored, and the bulk material removed during each time step is calculated from the instantaneous incursion depth and the proportion of the cell width traversed.

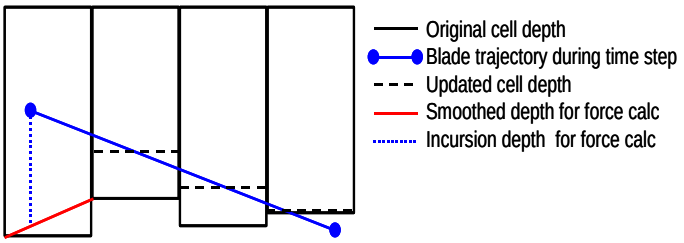

Fig 5: Update of liner cell depth during time step

The cell depth is updated to reflect the wear, but this is delayed until the blade has passed beyond the cell boundary to ensure that the full incursion depth is active while a blade is in transit through a cell. By accumulating the wear within a cell, the method automatically compensates for diagonal trajectories

through the cell, or where incursion is initiated or ceases part way though a cell – Fig 5.

Lateral wear forces are generated as a result of liner incursion. This consists of two components: a friction force due to rubbing and an impulse force due to the increase in momentum of the liner material following removal (wipeout force). The friction force is calculated using Coulomb friction, for which the friction coefficient used for wear, may be different from the value used for calculating direct rubbing with the casing. The impulse force arises due to the increase in momentum resulting from accelerating the liner material up to the blade tip speed, and is proportional to: the depth of incursion; the volume rate of removal; and the density of the liner material. The stagger angle of the blade is also important, as this determines the velocity change and direction of the ejected material – Fig 6.

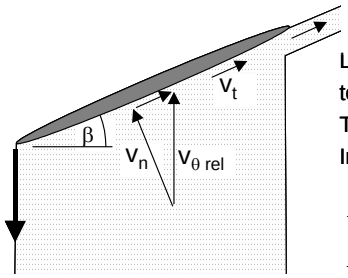

Liner Material ejected tangential to blade tip chord

Tang rel Velocity V_t retained

Impulse due to Normal Velocity V_n

$$F_\theta = -\rho c d V_{\theta rel}^2 \cos^2 \beta$$

$$F_z = -\rho c d V_{\theta rel}^2 \cos \beta \sin \beta$$

Fig 6: Liner Momentum – Staggered Blade

The impulse force (called the wipeout force) is different from the other contact forces considered, in that it is applied only to the blades, as the reaction force is considered to overcome the inertia of the virtual liner material and is therefore not transmitted to the engine casing. The method outlined above can be used to calculate the wipeout force under simulated ideal conditions, but may not be representative of the behaviour of real materials under rapid incursion conditions. If direct measurement data (or high quality simulation data) is available, then this can be used to define the wipeout force as a function of incursion depth and of blade tip speed, and this can be used directly in the simulation.

The axial hade angle of casing also has an influence on the snubbing behaviour. If the casing is conical, then relative axial, pitch, or yaw motion of the rotor, will reposition the axial contact position with respect to the casing, and will change the nominal clearance. Also, the resolved contact force will have a small axial component and this will induce yaw and pitching moments onto the rotor due to the high tip radius. These additional forces may influence the rotordynamic response of the rotor, resulting in further changes to the relative motion at the snubbing location.

Once the incursion depth and instantaneous liner removal rates have been established, the resulting forces can be calculated and interpolated onto the rotor and casing nodes as in the standard snubbing calculation.

Generally, for the case of non-uniform wear, the updating of the liner cell depth values, results in small steps in the liner depth as a blade moves from one cell into the next – Fig 5. The magnitude of these steps reduces as the number of cells is increased, but remains a finite value. This can give rise to convergence problems if a blade is positioned very close to a cell boundary at the end of a time step due to the step change in contact force during the next time step. Reducing the time step will exacerbate the problem, as the rate of change of contact force will increase. This is addressed by introducing a linear smoothing function for the last cell traversed within the time step (also indicated in Fig 5), which ensures that the contact force vary smoothly as the cell boundaries are approached. This smoothing is only applied to the calculated force at the end of the time step. It is not required, and should not be used when calculating the net material removed and the removal rate, as small errors will be introduced.

Similar convergence issues can occur at conditions where the liner is locally fully consumed, and the blade comes into direct contact with the casing. The change in friction coefficient results in an instantaneous change in the tangential forces. This is smoothed using a cubic smoothing function (Fig 7), which operates over a small proportion of the cell width to minimise errors, but which is effective in preventing critical time step reduction.

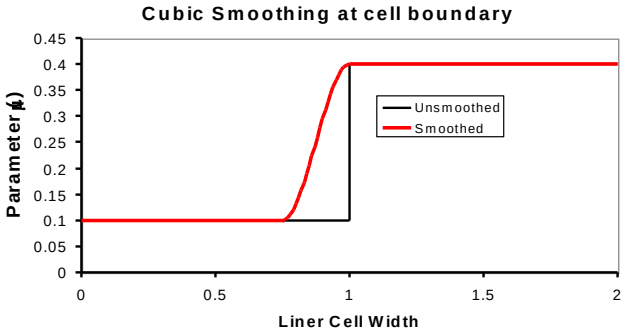

Fig 7: Cubic Smoothing function at cell boundary

Introduction of a dynamic blade model

In the models described so far, individual blades have been represented by inert non-linear springs. These have representative static radial stiffness, but do not have damping, and do not respond dynamically to the applied snubbing forces. In practice, transient and periodic vibration will be induced in the blades, which will in turn affect the contact behaviour. To address this, additional reduced models of either individual blades or of a full bladed assembly are introduced. The blade models are dynamically reduced to a small number of physical degrees of freedom at the tips of the blades.

The blade models are constructed such that they include speed specific properties (i.e. centrifugal stiffening), but are solved in the time domain calculation in a static reference frame. The blade models are incorporated into the global linear mass and stiffness matrices for the engine model, but form

discrete partitions with no physical connections between the respective blade and engine partitions. The interaction is provided purely by external forces representing the contact behaviour.

Blade casing contact is modelled as a two stage process. Firstly, the residual motion of each blade tip is transformed into the current angular position of the respective blade, and is added to the rotor motion. This transformation recognises the nominal position of each blade within the rotor and the integrated rotation of the shaft. Adding the blade motion to the rotor motion changes the effective position of the blade tip, and affects the angular position and intensity of snubbing as indicated in Fig 8.

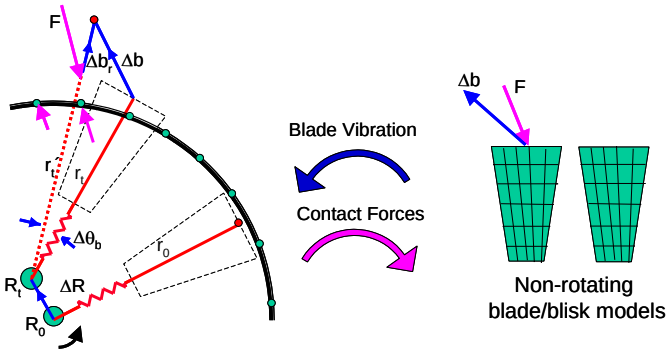

Fig 8: Interface between engine and blade models

Secondly, the snubbing forces are calculated using the revised blade tip positions. The snub forces are applied to the rotor and casing model and are also transformed back into the static frame and applied to the blade models, thereby inducing further blade motion.

The blade and casing models are linear, and have linear modeshapes. This will give rise to increasing errors at high amplitudes due to the limitations of small displacement assumptions (discussed later), and this may give rise to unrepresentative snubbing behaviour. However, the models are generally acceptable for blade displacements in the elastic range.

Implementation Issues

The features described in the above sections enable a comprehensive model of rotor stator interaction to be constructed including dynamic models of the rotor, casing, blade and liner, and enables the effects of multi-blade contact, plasticity and wear to be simulated. Not all of these features need to be used at the same time, and in the examples described next, some parts of the model are omitted.

IDEALISED TWELVE BLADE ROTOR EXAMPLE

This first example considers the interaction between an idealised bladed rotor and a rigid casing with a localised high spot at one position on the casing periphery -Fig 9.

The disk model is flexible, and as such the diametral modes are separated in frequency and can be readily identified from the frequency response characteristics. The FE bladed disc model contains 6204 tetrahedral elements and 38700 DOFs, but is dynamically reduced such that the analysis model contains only 2 master nodes on the tip of each blade (72 physical DOFs), and a further 30 generalised freedoms. The complete reduced model contains only 102 DOFs in total. However, an Eigen solution for the reduced model demonstrated that the modal frequencies were correct for the first three families of diametral modes, and the static stiffness of individual blade tips are also representative. The effects of centrifugal stiffening were not included for this idealised example as the consequent changes in frequency are not of interest.

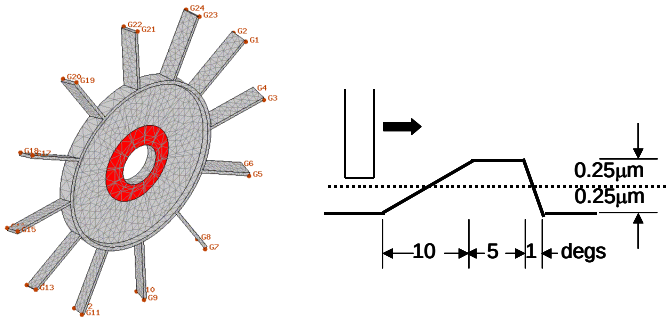

Fig 9: Idealised Bladed Disk and Casing Ramp Models

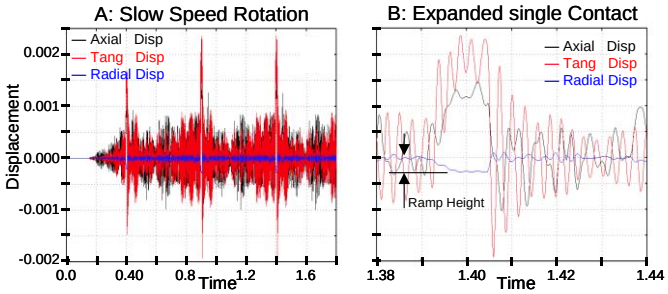

Fig 10: Blade tip response to casing ramp

Fig 10A plots the blade response for low speed rotation with contact active on each blade. The higher time resolution plot (Fig 10B) clearly indicates the shape of the ramp in the radial displacement, and the build up of much larger static deflection in the lateral and axial directions due to friction (drag displacement). This is released as the blade passes over the ramp, and the resulting transient response can be examined using Fourier Analysis to reveal the responding free modes.

Fig 11 shows that most of the first and second family modes can be identified from the response, the frequencies of which agree with the detailed FE analysis. The first family modes (edgewise mode) and second family (flap mode) are both excited due to the blade tip stagger angle. This initial example demonstrates that representative static and dynamic behaviour of the model is predicted, which is consistent with the properties of the unreduced modes, and with the excitation model.

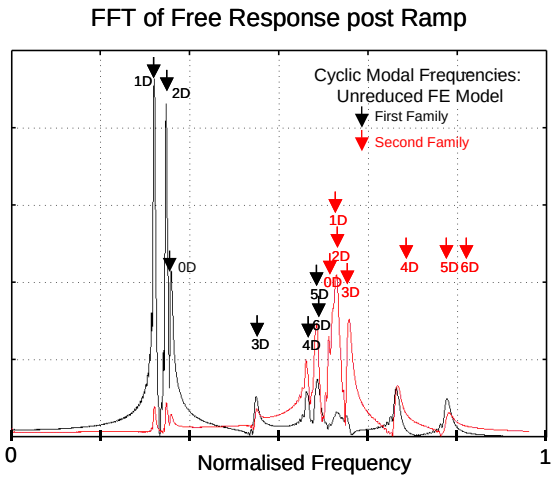

Fig 11: FFT of transient response to single contact

Fig 12 plots the response to a frequency sweep in the vicinity of the First Mode Third Engine order resonance.

For this example the speed of rotation is increased steadily over a five second period to enable the build up to resonance to be examined. The entire analysis represents approximately 270 revolutions and 3250 potential contacts with the ramp. The sweep rate and sweep range were optimised to minimise the effects of response lag and post resonance 'ringing', while retaining full resolution of the resonance peak, and minimising the analysis time. A frequency sweep rate normalised to the resonance frequency of 3.5% sec^{-1} was found to be suitable. The analysis takes approximately 6 minutes to solve on a 2.2GHz single processor PC.

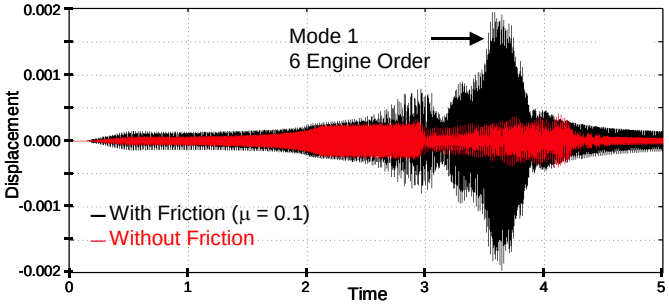

Fig 12: Mode 1, 6 Engine Order Resonance

Fig 12 compares the response with and without friction (μ=0.1), and demonstrates a large increase in peak response when friction is present. This is due to the increased drag displacement on the blade tips. The friction value used is low in comparison with test data, but has been selected to demonstrate the strong dependence on friction, and is not intended to be representative of genuine liner materials.

Fig 13 shows that the number of contacts increases as the amplitude increases near resonance. This is due to intermittent secondary contacts with the uniform cylindrical section of the casing. This occurs because for large lateral deflections, the effective clearance is reduced at the extremities of the vibration motion, and contact may therefore be induced.

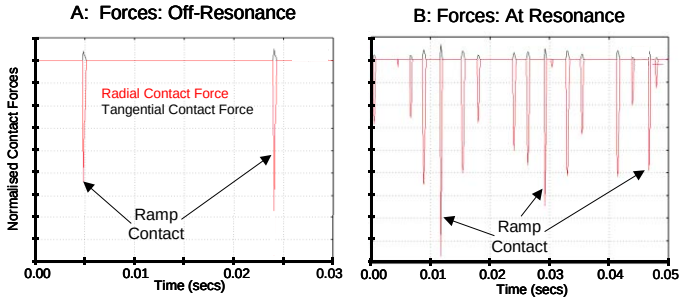

Fig 13: Secondary casing rubs near resonance

This effect is exaggerated for linear modeshapes, for which planer motion of the blade tip implies that an unrepresentative increase in the blade length occurs at high amplitude. In practice the tip trajectory at high amplitude will describe a shallow arc, and this will reduce the rate of incursion (Fig 14).

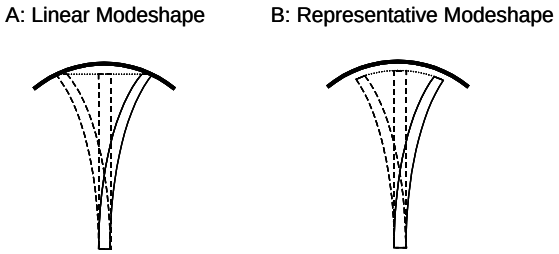

Fig 14: High amplitude modeshape errors

12 BLADE MODEL WITH LINER AND BLADE LEAN

A liner model is now introduced into the simulation. This is 2mm deep but is set up with a very low nominal clearance of 0.005mm. It is not possible to introduce a ramp into a liner model or a uniform misalignment, as this will wear away in the early stages of the interaction, and no information will be gathered at what might be more interesting speed conditions. It is also not feasible to start the simulation at resonance as some degree of frequency stiffening might take place, and is then necessary to track the development of resonance from a lower speed off-resonance condition. To address these issues, a casing model was introduced for which a small annular segment advances inwards at a slow but constant rate. The liner model, taking its clearance datum from the casing, advances locally at the same rate, presenting a small depth of fresh liner material to each passing blade. This may or not be removed depending on the blade motion - Fig 16. Note that this method of exciting the blade is not intended to be representative of conditions a blade would experience in practice, but is a convenient method for ensuring consistent low level interaction over a wide frequency. The alternative is to introduce a strong preferential initial clearance pattern, which might influence the resulting behaviour.

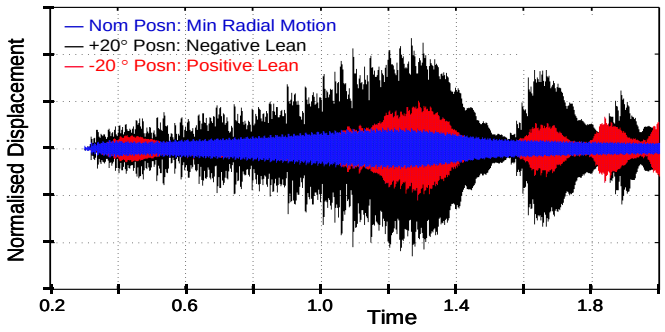

Fig 15: Effect of Radial Modeshape on Response

The influence of aerofoil tip lean was also introduced into this example. For real blades, the tip modeshape may not be planar, but may include some radial motion due to lean and stagger of the aerofoil. Consequently, the clearance will vary periodically with blade vibration. The phase of the tip motion may influence the severity of the interaction. For example, if the radial motion is increasing while the tip is moving in the direction of rotation, then the tip might have a tendency to 'dig in' to the casing. Conversely, if the maximum occurs when the tip is moving rearwards, then the frictional drag might be increased. Increased radial motion of the idealised blade model can be synthesised by specifying a small misalignment in the orientation of the disk, such that a small proportion of the planer tip motion is misinterpreted as radial motion following transformation to the rotating coordinate frame. It is not necessary to modify the input model to achieve this, as a parameter is available in the code to align the blade model/s with the rotor motion at the start of the analysis. Fig 15 compares the response for different levels of misalignment. This shows that the response is significantly higher for both positive and negative lean, but is highest for positive lean. The response is much nosier for the misaligned blade and there is evidence of other modes being excited.

FULL CHORD TIP RUB EXAMPLE

The final example is based on an early design standard of compressor blade aerofoil for which tip rub induced blade damage accompanied by high liner wear has occurred in isolated incidents. The liner wear tends not to be uniform, but has been associated with a dominant 6 lobed wear pattern. This design is compared with an improved design that is known to be more tolerant, but no quantitative measurement results are available for either example. It was therefore necessary to devise a set of liner parameters (density, incursion rate, rotation frequency and acceleration rate) which are consistent with expected engine conditions, and for which the initial blade design is marginally unstable. The increase in stability margin of the redesigned blade can then be used as a measure of the improved tolerance to rubs. The analysis model consisted of a single blade earthed on the root mating surfaces – Fig 16.

This is a design standard model including CF stiffening equivalent to the resonant speed condition. The model was CMS reduced to the 6 aerofoil nodes shown in Fig 16 and included a further 100 generalised variables. The shaft and casing were represented as inert rigid structures, as there was no evidence of a rotordynamic influence on the behaviour. A concentric liner with tight clearance was modelled, which included a localised advancing high spot as described previously. For this high-speed excitation condition, the wipeout inertia forces are very much higher than the liner penetration and friction forces, which were therefore not included in the analysis for clarity. The following analyses are not intended to be representative of particular engine conditions, but are chosen to explore potential conditions under which instability may arise.

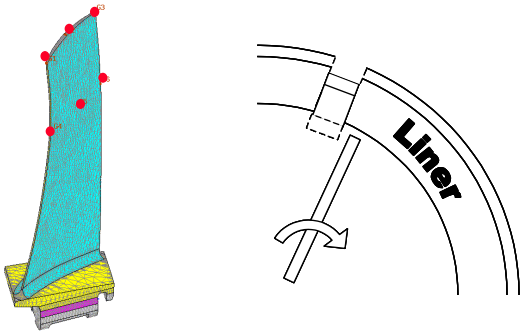

Fig 16: Discrete blade and liner high spot models

Initial analysis runs were carried out with the snub active at selected positions on the blade tip in isolation: Leading Edge (LE), Mid-Chord (MC) and Trailing Edge (TE). These results showed that the maximum dynamic incursion occurs at the Trailing Edge, but the maximum overall response occurs with Mid-Chord excitation (Fig 17). No clear resonance is observed for LE excitation, implying that damping is increased.

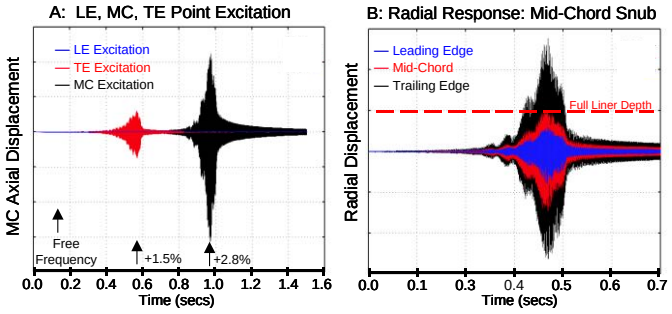

Fig 17: LE, MC & TE Snub sensitivity

These results show that the resonant speed is different for each snub location, and for all cases is higher than the expected resonance condition for free vibration. This demonstrates the frequency stiffening effect of liner wear, and also demonstrates the difficulty in selecting a suitable speed for a single speed analysis. The reduced model was not updated to reflect the increased CF stiffening applicable at the increased resonant speed, as this was not considered to be significant for a 2.8% increase in speed. Where larger speed changes are encountered, the linear model would be revised at each speed condition by

interpolating between two reduced models derived at a high speed and zero speed conditions. The interpolation would be conducted using a square law interpolation rule. In addition the resultant interpolated stiffness matrix would be scaled by a further non-linear speed dependent factor representing the approximate effect of temperature on the Young's Modulus of the blade material.

A more representative analysis was set up by applying independent snubs to all three blade tip positions simultaneously. All snubs were set to the same clearance value, and the orientation of each node was set to be representative of the stagger of the blade, i.e. the nominal Trailing Edge contact occurs at an angular position 5.8° clockwise relative to the Leading Edge. The high spot excitation was restricted to the mid-chord position, but contact across the full chord occurs with increasing blade vibration due to the increasing radial motion of the blade tip. The severity of the resultant blade response was controlled by increasing the density of the liner material over a range of arbitrary but representative values.

The frequency and amplitude of the resonant response were observed to increase steadily with density up to a critical value. Beyond this value, the response becomes unstable, and was predicted to rise rapidly with speed (Fig 18).

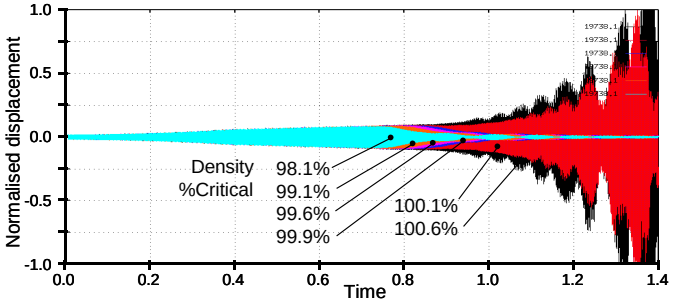

Fig 18: Onset of instability with increasing density

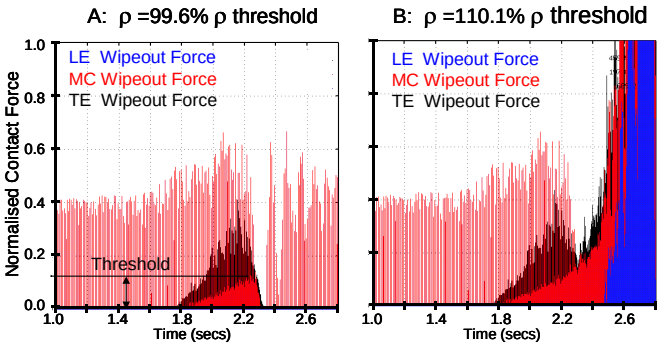

Fig 19: Blade Tip Wipeout Forces

Fig 19 shows the corresponding contact forces at the three tip positions for density values slightly below and above the threshold condition. This shows similar behaviour during the approach to resonance. Contact is initially restricted to the mid-chord position, and consists of a single pulse each time the blade traverses the high spot on the casing. Closer to resonance, additional intermittent contact is observed, the magnitude of which is less than the high spot contact forces, and does exceed 25% of the ramp force (MC position). Intermittent contact is initiated on the TE slightly earlier than at the MC position, and is higher in amplitude, due to the increased radial motion in the modeshape. For the low density result, the amplitude collapses above resonance - this being typical of amplitude stiffening systems - and all contact forces cease for a short period during the collapse. The behaviour at the higher density condition, shows an indication of the start of the amplitude collapse, but contact at the MC position is maintained and continues to grow. An exponential rise in the response occurs following this point, which is only interrupted when the full liner depth has been eroded. The results at these high amplitude conditions are unreliable however as the assumption of linear modeshapes becomes increasingly unrepresentative. In practice, the radial component of motion will reduce once the blade is fully untwisted, and this will limit the ultimate depth of incursion. The modeshape assumptions should, however, be suitable at the onset of instability.

Fig 20 shows the liner wear for half the casing at various times during the approach to instability. This shows the development of a lobed pattern (6 lobes for the whole casing). With increasing speed and amplitude, this pattern advances such that the blade is always confronted with fresh full depth liner material. Consequently, the rubbing forces increase proportionately with amplitude, and this helps to sustain the exponential growth in the response. This advance through the liner material is due to the phase change in the forced response approaching resonance. This phase advance is dependent on increasing rotor speed, and the instability collapses if the increase in shaft speed is not maintained. Similarly, instability only occurs with increasing shaft speed. During deceleration, the combination of amplitude stiffening and reducing speed, moves the response further from resonance. An amplitude jump will occur, but this will be to a stable pre-resonance condition.

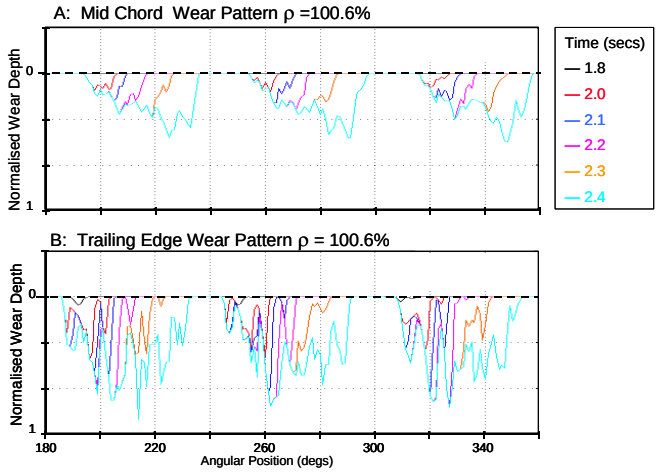

Fig 20: Development of 6D Liner Wear Pattern

Fig 20B shows the equivalent wear on the Trailing Edge. This retains the 6 lobed pattern, but is deeper and is more ragged. The spiky appearance is due to the excitation of higher

frequency modes, which are more active, at the tip edges. These modes can lead to radial cracks developing in the tip of the blade.

Repeat analysis on redesigned blade

The above analysis was repeated for the redesigned blade, which has similar frequencies, but reduced lean. This blade has a proven tolerance to tip rubs. The frequency rise during snubbing is much reduced for this standard of blade, and much higher densities can be tolerated, before instability is initiated – Fig 21.

The real improvement may be much higher however, as at high amplitude conditions, the linear modeshape assumptions are less reliable, and liner contact results from the planar tip motion intersecting with the curved casing. In practice, the tip motion will follow an arc and may not contact the casing at high amplitude – Fig 14.

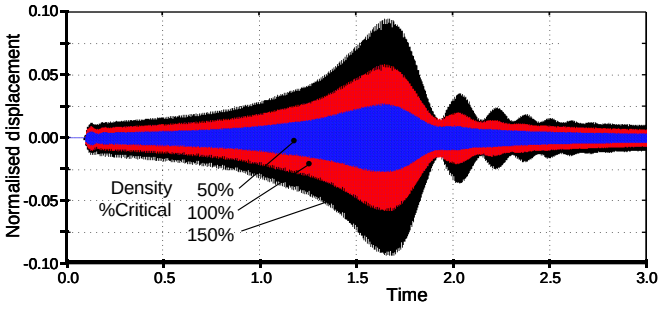

Fig 21: Liner Snub Response: Redesigned Blade

Conclusions

A method has been demonstrated for predicting the complex behaviour of rub induced blade vibration in conjunction with an eroding liner. The analysis is a time marching analysis conducted in a stationary reference plane, but blade rotation is simulated by exchanging forces and displacements via a continuously variable transformation.

Physical descriptions have been provided of the various enhancements that have been added to a standard centreline snubbing model to facilitate the full multi-blade capability. These enhancements have been demonstrated using idealised models run at low speed, for which the behaviour can be verified intuitively.

By using highly reduced models of the casing and rotor structures it has been possible to run analyses at representative speeds and for sufficiently long periods of simulated time, to determine the resonant response, and any associated amplitude stiffening, sweep rate dependencies, induced transients, etc. It has also been possible to validate the quality of the reduced model in terms of frequencies, dynamic and static stiffness, etc, by observing the low speed free response to an isolated rub.

The method has been applied to real blade examples, where it successfully predicts representative observed liner wear behaviour patterns and ranks the rub tolerance for alternative designs correctly.

The limited testing has identified that short duration instability may occur, but is dependent on particular conditions being met simultaneously, i.e. the snub must be severe, but must be initiated sufficiently close to resonance that the incursion zone on the liner is not eroded before the response becomes established. Similarly, the excitation frequency (engine speed) must be increasing, but the acceleration rate is also important. If the acceleration rate is too slow, then the angular advance through the liner will reduce and the wipeout forces may be insufficient to sustain the increase in response, and if it is too fast, then resonance will be traversed before the response becomes established. The analysis has also demonstrated that radial vibration response in the fundamental modes has a strong influence on the response, but more is not always worse, the distribution across the chord is also important, as is the phase with respect to the lateral components of the modeshape.

The main strength of the approach described in this paper is that it is low cost, and therefore enables large numbers of 'what if' scenarios to be tested. It is possible to determine the various types of behaviour that could be excited under highly conducive conditions; it enables rub tolerant design features to be identified; and it enables the rub tolerance of new and existing designs to be compared.

REFERENCES

[1] Padova C, Barton J, Dunn, and Manwaring S,. "Experimental results from controlled blade tip/shroud rubs at engine speed" ASME Journal of Turbomachinery, 129, pp.713-723, 2007

[2] Ferguson J, Dunn M, Padova C, Manwaring S, Turner, A, "A moving load finite element based approach to determination of case load in a blade-on-casing incursion", GT2010-22048 Proceedings of ASME Turbo Expo 2010, June 2010, Glasgow.

[3] Turner K, Dunn N, Padova C, "Aerofoil deflection characteristics during rub events", GT2010-22048 Proceedings of ASME Turbo Expo 2010, June 2010, Glasgow.

[4] Craig. R.R., 1987, A review of time-domain and frequency domain component-mode synthesis methods", J. of Modal Analysis, 1987, April,pp.59-72

[5] R J Williams, 2004, "Parametric characterization of rub induced whirl instability using an instrumented rotordynamics test rig" Proceedings of 8th IMechE Vibrations in Rotating Machinery Conference 651-660

[6] Petrov, E.P., Ewins, D.J., 2003, "Analytical formulation of friction interface elements for analysis of nonlinear multi-harmonic vibrations of bladed discs", ASME J. of Turbomachinery, Vol.125, April,pp.364-37